ALTERNATIVE MODELS OF THE DOUBLY-FED INDUCTION MACHINE FOR POWER SYSTEM DYNAMIC ANALYSIS

Koch, F., Shewarega, F. and Erlich, I.
University of Duisburg-Essen, Institute of Electrical Power Engineering and Automation, *D-47057 Duisburg, Germany*

Abstract –The paper focuses on the suitability of alternative models of the doubly-fed induction machine (DFIM) for the study of crowbar action. The quasi-stationary model disregards the fundamental frequency transients in the machine currents and, as a result, can lead to incorrect prediction of the sequence of crowbar actions, whereas the detailed simulation of the entire network is computationally unfeasible. For studies focussing primarily on the influence of the DFIM on the interconnected system, the quasi-stationary model can still be used. For the detailed study of the machine transients, however, the fifth order model with the rest of the network represented by a single-machine operating on an infinite bus is necessary. Simulation results have revealed that the crowbar does not significantly affect the real power output of the machine during fault. However, the effect of the crowbar on the reactive power is more pronounced, particularly the second switching that may take place after fault clearance. This situation can impede the post-fault voltage recovery process in the network and has to be considered undesirable from the point of view of the network.

Keywords – Crowbar, Induction generators, Power systems, Transient stability, Wind power generation.

INTRODUCTION

Wind power generation has experienced a rapid growth in the recent past. Within a space of a decade large multi megawatt units have become commonplace. This fact raises a range of operational issues, which previously were not of interest due to the limited ability of the small wind turbines scattered over a wide geographic area to affect the overall system performance in any significant way. The protection system of such small units was designed with merely self-protection in mind. In the event of a major fault in the network, for example, wind units can disconnect themselves from the network and shut down, leaving the task of dealing with the fault and its aftermath to the conventional plants in the interconnected system.

In light of the ever increasing share of the wind power in the overall electric energy supply and the size of the individual units (already in use or under development), this sort of allocation of duties is becoming increasingly untenable [1]. Accordingly, many power utilities have found it necessary to issue guidelines for the interconnection of wind turbines with the public grid

setting out the requirements, which the wind units have to fulfil during normal operation and fault conditions [2].

The increased significance and diffusion of wind units together with the upcoming new responsibilities vis-à-vis the grid calls for new control and design concepts that would put the wind generators in a position to respond to these needs in parallel operation with the conventional plants. This fact necessitates a deeper understanding of the dynamic interaction of wind turbines with the interconnected system.

This paper focuses on the modelling of the doubly-fed induction machine in the context of its application as a generator in variable speed wind turbines and its implication on the results of fault simulation.

MATHEMATICAL MODEL OF THE INDUCTION MACHINE

The induction generator is the most commonly used device for wind power generation. The two basic alternatives are the squirrel-cage type operating on a stall-controlled wind turbine and the doubly-fed slip-ring machine. These two types are also referred to as fixed speed and variable speed machines, respectively. In a fixed speed machine, the no-load speed of the machine is determined by the grid frequency and design parameters, and the speed is so chosen that the wind energy at the expected local wind speed can be optimally exploited. During normal operation of the machine, the speed varies within a narrow band in the super-synchronous range. In a fully variable speed machine, however, the speed range may vary somewhere between -50% to +25% of the synchronous speed. The power electronic equipment provides a variable rotor voltage that is adjustable both in magnitude and phase angle. As a result, the rotor speed can be varied to match the optimum operating point in the power-efficiency curve at any practical wind speed. This capability of the machine to change its speed as necessary can lead to an increase in annual energy production of up to 5% [3].

Before the simulation results of a short circuit in the network obtained using the alternative induction machine models are discussed the general mathematical relationships governing the electromechanical energy conversion process will be summarized.

Fifth order model

Equations (1)-(5) represent the complete set of mathematical relationships that describe the dynamic behaviour of the machine. The superscript $\angle K$ denotes an arbitrary reference frame rotating at the speed $\omega_{K.}$ (If ω_K is chosen to be ω_0, the

voltage, current and flux linkage space-phasors correspond to the familiar complex phasors.)

Voltage equations:

$$\underline{u}_S^{\angle K} = r_S \cdot \underline{i}_S^{\angle K} + \frac{d\underline{\psi}_S^{\angle K}}{dt} + j \cdot \omega_K \cdot \underline{\psi}_S^{\angle K} \qquad (1)$$

$$\underline{u}_R^{\angle K} = r_R \cdot \underline{i}_R^{\angle K} + \frac{d\underline{\psi}_R^{\angle K}}{dt} + j \cdot (\omega_K - \omega_R) \cdot \underline{\psi}_R^{\angle K} \qquad (2)$$

Flux linkages:

$$\underline{\psi}_S^{\angle K} = l_S \cdot \underline{i}_S^{\angle K} + l_h \cdot \underline{i}_R^{\angle K} \qquad (3)$$

$$\underline{\psi}_R^{\angle K} = l_h \cdot \underline{i}_S^{\angle K} + l_R \cdot \underline{i}_R^{\angle K} \qquad (4)$$

with $l_S = l_h + l_{\sigma S}$ and $l_R = l_h + l_{\sigma R}$

Equation of motion:

$$\frac{d\omega_R}{dt} = \frac{1}{T_m}\left(m_T + \frac{k_R}{l'} \cdot \mathrm{Im}\left\{ \underline{\psi}_S \cdot \underline{\psi}_R^* \right\} \right) \qquad (5)$$

where $l' = l_h + l_{\sigma S} - \frac{l_h^2}{l_h + l_{\sigma R}}$ and $k_R = \frac{l_h}{l_h + l_{\sigma R}}$.

The nomenclature of all symbols used in the above equations and the equations to follow are given at the end of the paper.

Equations (1) and (2) resolved into real and imaginary parts together with the equation of motion (5) constitute the 5th order model of the doubly-fed induction machine. The terminal voltage $\underline{u}_S^{\angle K}$ forms the link to the rest of the network.

Quasi-stationary model (third order model)

The quasi-stationary model is derived under the assumption that the transformer voltage in the stator winding can be neglected against the much greater speed voltage, i.e.

$$\left| j\omega_K \cdot \underline{\psi}_S^{\angle K} \right| \rangle\rangle \left| \frac{d\underline{\psi}_S^{\angle K}}{dt} \right| \qquad (6)$$

Resorting to the network coordinates (choosing a reference frame rotating at a constant speed corresponding to the network radian frequency ω_0) and using the

familiar notation for voltage and current phasors, we obtain from (1) for the stator flux linkages:

$$\underline{\psi}_S = \frac{\underline{u}_S - r_S \cdot \underline{i}_S}{j\omega_0} \qquad (7)$$

By substituting (4) into equation (3), the rotor current can be eliminated to yield:

$$\underline{\psi}_S = l_S \cdot \underline{i}_S + \frac{l_h}{l_R} \left(\underline{\psi}_R - l_h \cdot \underline{i}_S \right) \qquad (8)$$

Equating equations (7) and (8) results in:

$$\underline{u}_S - r_s \cdot \underline{i}_S = j\omega_0 \left(l_S \cdot \underline{i}_S + \frac{l_h}{l_R} \cdot \left(\underline{\psi}_R - l_h \cdot \underline{i}_S \right) \right) \rightarrow$$

$$\underline{u}_S = \left(r_S + j\omega_0 l' \right) \underline{i}_S + j\omega_0 k_R \underline{\psi}_R \qquad (9)$$

The voltage equation (9) corresponds to the following equivalent circuit.

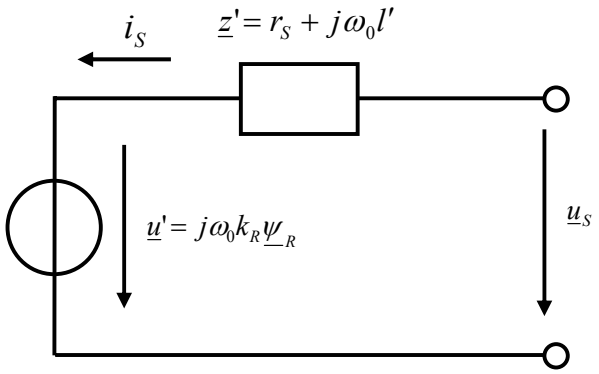

Figure 1: Quasi-stationary equivalent circuit of the induction machine

The internal voltage in Figure 1 ($\underline{u}'$) is a function of the rotor flux, which is a state variable. Substituting (4) into (2), the rotor flux can now be brought to the state-space form:

$$\begin{aligned}\frac{d\underline{\psi}_R}{dt} &= -\left(\frac{r_R}{l_R} + j\cdot(\omega_0 - \omega_R)\right)\cdot\underline{\psi}_R + k_R\cdot r_R\cdot\underline{i}_S + \underline{u}_R \\ &= -\left(\underline{T}_{L0}^{-1} + \frac{j\cdot\omega_0\cdot k_R^2\cdot r_R}{\underline{z}'}\right)\cdot\underline{\psi}_R + \frac{k_R\cdot r_R}{\underline{z}'}\cdot\underline{u}_S + \underline{u}_R\end{aligned} \qquad (10)$$

where $\underline{T}_{L0}^{-1} = \frac{r_R}{l_R} + j\cdot(\omega_K - \omega_R)$ and $\underline{z}' = r_S + j\omega_0 l'$

Equation (10) together with the following equation of motion constitute the quasi-stationary model of the induction machine.

$$\frac{d\omega_R}{dt} = \frac{1}{T_m}\left(k_R\cdot\mathrm{Im}\left\{\underline{i}_S\cdot\underline{\psi}_R^*\right\} + m_T\right) \qquad (11)$$

The determination of the rotor flux linkages $\underline{\psi}_R$ and thus the stator current $\underline{i}_S$ requires the numerical integration of (10) and (11) and the solution of the load flow equations of the network on which the machine is operating in an alternating process.

It should be noted at this point that the mathematical relationships are valid for both induction machine types in equal measure, with the only modification being that for the squirrel-cage machine the rotor voltage ($\underline{u}_R$) needs to be set zero.

The steady state model

Before the discussion of the dynamic models is pursued further, the steady-state performance of the machine will be reviewed briefly with the objective of identifying the range of control options and the operational capabilities of the machine.

Neglecting the transformer voltages in (1) and (2) and in network co-ordinates:

$$\underline{u}_S = r_S\underline{i}_S + j\omega_0\underline{\psi}_S \qquad (12)$$

$$\underline{u}_R = r_R\underline{i}_R + j(\omega_0 - \omega_R)\underline{\psi}_R \qquad (13)$$

Eliminating the flux linkages using equation (3) and (4), we obtain:

$$\begin{aligned}u_S &= r_S\underline{i}_S + j\omega_0\cdot(l_S\underline{i}_S + l_h\underline{i}_R) \\ &= r_S\underline{i}_S + jx_S\underline{i}_S + jx_h\underline{i}_R\end{aligned} \qquad (14)$$

$$\frac{\underline{u}_R}{s} = \frac{r_R}{s}\underline{i}_R + j\omega_0 \cdot (l_h \underline{i}_S + l_R \underline{i}_R) = \frac{r_R}{s}\underline{i}_R + jx_h \underline{i}_S + jx_R \underline{i}_R \qquad (15)$$

with $s = \dfrac{\omega_0 - \omega_R}{\omega_0}$

Equations (14) and (15) can also be illustrated using the equivalent circuit given in Figure 2.

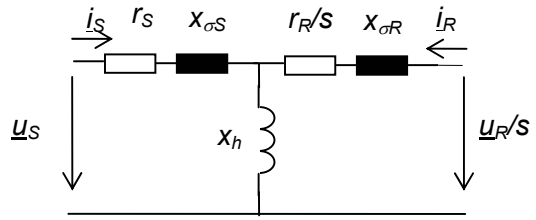

Figure 2: Equivalent circuit of the doubly-fed induction machine in steady-state

Equations (14) and (15) can then be written in a matrix form and used (after matrix inversion) to express the stator and rotor currents in terms of stator and rotor voltages.

$$\begin{pmatrix} \underline{i}_s \\ \underline{i}_R \end{pmatrix} = \begin{pmatrix} \underline{y}_{11} & \underline{y}_{12} \\ \underline{y}_{21} & \underline{y}_{22} \end{pmatrix} \cdot \begin{pmatrix} \underline{u}_s \\ \underline{u}_R / s \end{pmatrix} \qquad (16)$$

Electromagnetic torque, real and reactive power

The electromagnetic torque developed by the machine as well as expressions for the real and reactive power is derived using the following power relationship:

$$\underline{S} = \underline{u}_S \cdot \underline{i}_s^* + \underline{u}_R \cdot \underline{i}_R^* \qquad (17)$$

Substituting the relationships (1) and (2) for the stator and rotor voltages in (17):

$$\begin{aligned} \underline{S} &= \underline{i}_S^* \cdot \left(r_S \underline{i}_S + \frac{d\underline{\psi}_S}{dt} + j\omega_0 \underline{\psi}_S \right) + \underline{i}_R^* \cdot \left(r_R \underline{i}_R + \frac{d\underline{\psi}_R}{dt} + j(\omega_0 - \omega_R)\underline{\psi}_R \right) \\ &= r_S \cdot \left|\underline{i}_S\right|^2 + r_R \cdot \left|\underline{i}_R\right|^2 + j\omega_0 (\underline{\psi}_S \cdot \underline{i}_S^* + \underline{\psi}_R \cdot \underline{i}_R^*) - j\omega_R \underline{\psi}_R \cdot \underline{i}_R^* \qquad (18) \\ &\quad + \left\{ \frac{d\underline{\psi}_S}{dt} \cdot \underline{i}_S^* + \frac{d\underline{\psi}_R}{dt} \cdot \underline{i}_R^* \right\} \end{aligned}$$

The last term in equation (18) (representing the change in magnetic field energy) can be neglected in steady-state. After eliminating the flux linkages using the appropriate relationships in equations (3) and (4), we get:

$$\begin{aligned}\underline{S} &= r_S \cdot \left|\underline{i}_S\right|^2 + r_R \cdot \left|\underline{i}_R\right|^2 \\ &+ j\omega_0 \cdot l_S \cdot \left|\underline{i}_S\right|^2 + j\omega_R \cdot l_R \cdot \left|\underline{i}_R\right|^2 + j\omega_0 \cdot l_S \cdot \underline{i}_S^* \cdot \underline{i}_R + j\omega_0 \cdot l_h \cdot \underline{i}_S \cdot \underline{i}_R^* \quad (19) \\ &- j\omega_R \cdot l_R \cdot \underline{i}_S \cdot \underline{i}_R^* - j\omega_R \cdot l_R \cdot \left|\underline{i}_R\right|^2\end{aligned}$$

After re-arranging and introducing the slip (s), we get:

$$\underline{S} = \underbrace{(r_s + jx_S) \cdot \left|\underline{i}_S\right|^2 + (r_R + jx_R \cdot s) \cdot \left|\underline{i}_R\right|^2}_{P_L + jQ_L} + \underbrace{jx_h \cdot \underline{i}_S^* \cdot \underline{i}_R + jx_h \cdot s \cdot \underline{i}_S \cdot \underline{i}_R^*}_{P_G + jQ_G} \quad (20)$$

where $\underline{S}$ is the complex power at the terminals of the machine, $P_L + jQ_L$ represent the losses and the reactive power consumed by the machine. $P_G + jQ_G$ describes the internal active and reactive power generation.

Separating the internal power term into its real and imaginary components results in:

$$P_G = \mathrm{Im}\left\{x_h \cdot (1-s) \cdot \underline{i}_S \cdot \underline{i}_R^*\right\} \quad (21)$$

$$Q_G = \mathrm{Re}\left\{x_h \cdot (1+s) \cdot \underline{i}_S \cdot \underline{i}_R^*\right\} \quad (22)$$

$$T = \frac{P_G}{\omega_R} = \mathrm{Im}\left\{l_h \cdot \underline{i}_S \cdot \underline{i}_R^*\right\} \quad (23)$$

It is now a straightforward procedure to relate the power and torque relationships ((21)-(23)) to the magnitude and phase angle of the rotor voltage by using (16).

The expression for the electromagnetic torque, for example, is:

$$T = \alpha_T \cdot \left(\frac{u_R}{s}\right)^2 + \beta_T \cdot \cos(\vartheta - \delta_T) \cdot \frac{u_R}{s} + \gamma_T \quad (24)$$

where ϑ is the difference between stator and rotor voltage phase angles. The other coefficients (α_T, β_T, δ_T and γ_T) (defined in the appendix) are functions of the terminal voltage and machine parameters, and, as a result, remain constant when the machine operates on a constant voltage bus.

Similar expressions can be given for P_G and Q_G. γ_T (in (24)) corresponds to the induction torque and is independent of the rotor voltage. On the other hand, the induction torque term (γ_T) is zero when the machine runs at synchronous

speed. The torque at the synchronous speed (the synchronous torque) can be obtained by setting $s = 0$ in (16).

$$T_{syn} = \alpha_{Syn} \cdot \left(\frac{u_R}{s} \right)^2 + \beta_{Syn} \cdot \cos(\vartheta - \delta_{Syn}) \cdot \frac{u_R}{s} \quad (25)$$

Operational capabilities

As a result of the applied rotor voltage, the machine is capable of operating at over-synchronous, sub-synchronous or synchronous speeds as a generator. The real and reactive power outputs of the machine in relation to rotor voltage phase angle with the rotor voltage magnitude as a parameter are given in Figure 3 and 4. The figures demonstrate the capability of the machine to operate in all four quadrants.

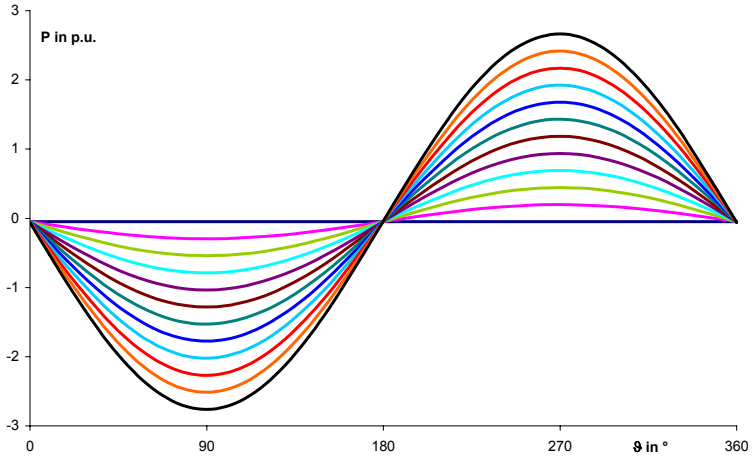

Figure 3: Real power as a function of the rotor voltage phase angle

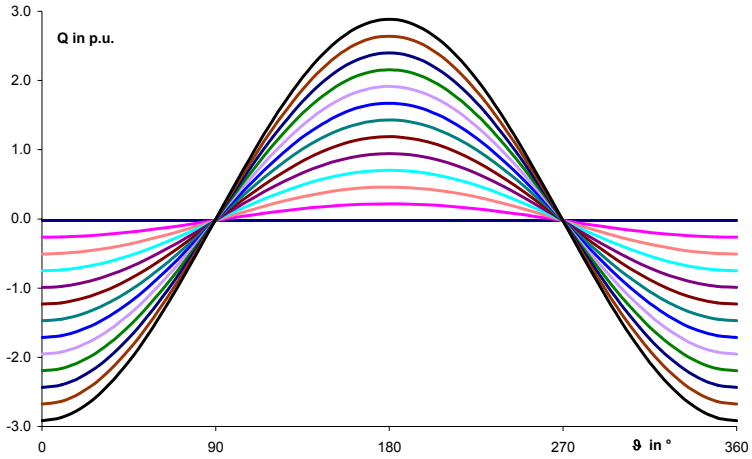

Figure 4: Reactive power as a function of the rotor voltage phase angle

TRANSIENT ANALYSIS OF THE DOUBLY-FED INDUCTION MACHINE

Fifth order versus third order models

It has been a common practice to represent the induction machine using its quasi-stationary model in power system transient simulations. The results obtained using this model proved to be satisfactory for most applications. The need to revisit the issue, i.e. the discussion as to the adequacy of the quasi-stationary model to represent the induction machine in transient studies or not, has been prompted by the emerging requirement on the wind plants not to disconnect themselves from the grid in the event of fault. It will be recalled that a salient feature of the DFIM is the fact that it contains a pulse-width modulated converter in its rotor, which enables the control of the magnitude and phase angle of the rotor voltage. If the DFIM is not to be disconnected from the network during fault, as can be foreseen from the tenor of current discussions, the rotor-side converter needs to be protected against excessive currents that might arise as a result of the fault. One such protection scheme is the by-passing of the converter and the connection of the rotor circuit to external impedance in the so called crowbar protection.

The main objective of this study was to use these two alternative models (the quasi-stationary model and the more detailed 5^{th} order model) to compute the rotor current during a major fault and assess the significance of the reduced accuracy as a result of the use of the quasi-stationary model and its implication

on the programming of crowbar actions. Using the model developed, currents in the converter during fault and at converter blocking followed by connection to the crowbar, the effect of the crowbar impedance on the fault current, etc. can all be studied. Furthermore, the impact of crowbar switching and then the re-instatement of the rotor-side converter on the real and reactive power output of the machine can be computed.

Test system

The test system, shown in Fig.5, comprises of a doubly-fed induction machine connected to a grid via a transformer. Additionally, the stator-side and rotor-side converters together with their control systems have been simulated in detail. The IGBT is implemented by a macro model without taking into account either the geometry of the device or the complex physical processes.

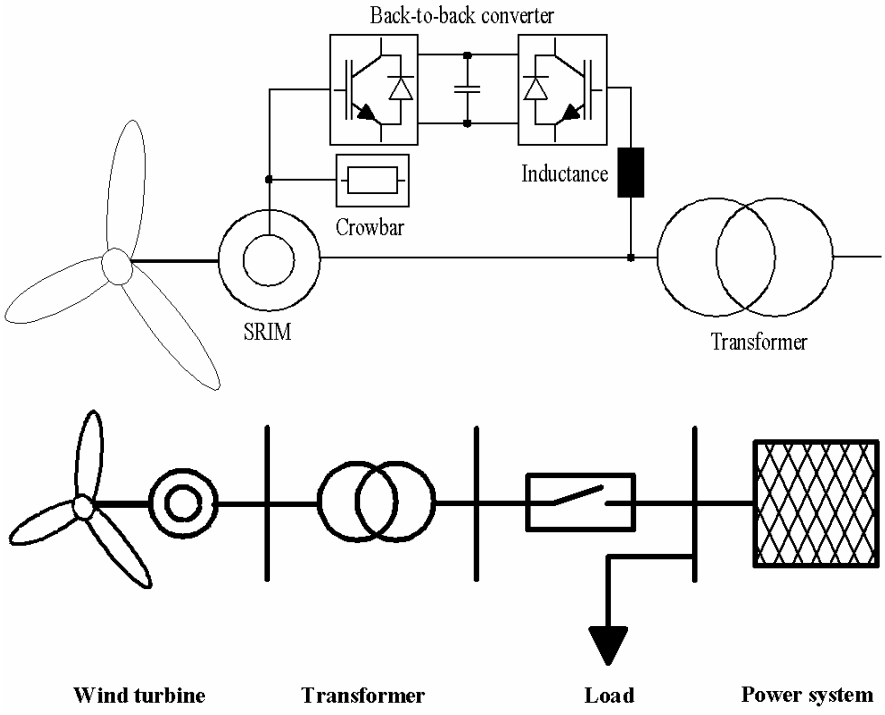

Figure 5: The Test System

The simulated scenario

A symmetrical three-phase fault of 150 ms duration is introduced at the network bus bars on the high voltage side of the transformer. The fault impedance is so chosen that the terminal voltage at the fault location is reduced to 20% of its pre-fault value. The crowbar logic is adjusted in such a way that each time during the course of the fault the rotor current exceeds a certain threshold value, the rotor-side converter blocks and the rotor terminals are connected to one another through the crowbar (pure resistance in this study). It was found out from a manufacturer's catalogue that the IGBT is capable of withstanding a current magnitude twice the rated current for a time span of no more than 1 ms [4]. On the basis of this information and the ratings of the machine simulated in this study, a crowbar switching takes place when the rotor current exceeds 1.8 p.u. The crowbar has a resistance equal to 50 times the rotor resistance [5]. After the preset time interval of 100 ms elapses the crowbar is removed and the original configuration of the rotor circuit is restored.

Results of the simulation

Figures 6 and 7 show the real and reactive power outputs of the machine during fault. As expected, the third order model does not account for the oscillatory 50-Hz component superimposed on the quasi-stationary component and describes only the average pattern. Since the rotor cannot follow the fast oscillations, the quasi stationary model reflects the electromechanical transient process fairly accurately.

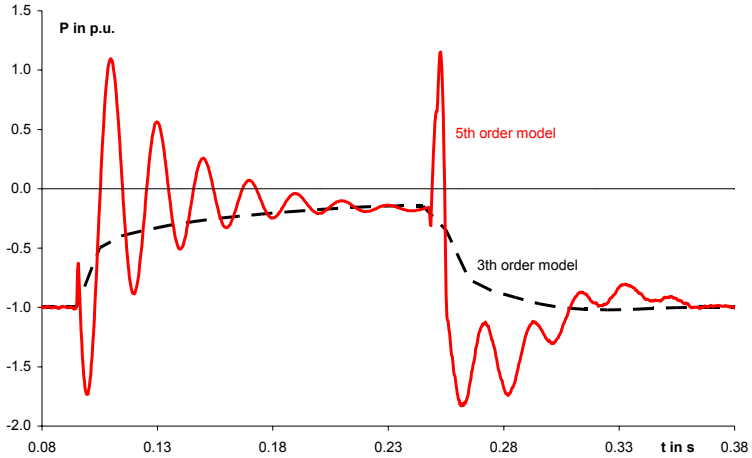

Figure 6: Comparison of real power output obtained using 3rd and 5th order model

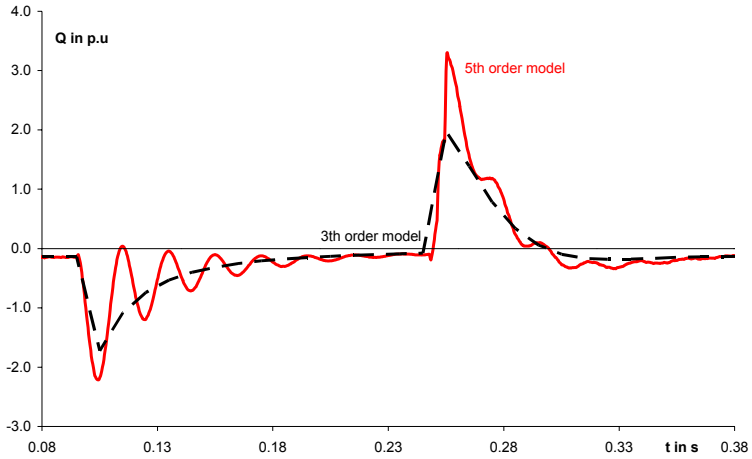

Figure 7: Comparison of reactive power output obtained using 3rd and 5th order models

More interesting in this study, however, was to find out how the crowbar action affects the real and reactive power outputs of the machine as well as the rotor currents in each phase of the machine. The results obtained are summarized in Figures 8 – 10. The pulse-shaped solid line in Figures 8 and 9 indicates the timeframe of crowbar action, i.e. a value of "1" implies the crowbar is switched on or else the rotor is connected to the converter.

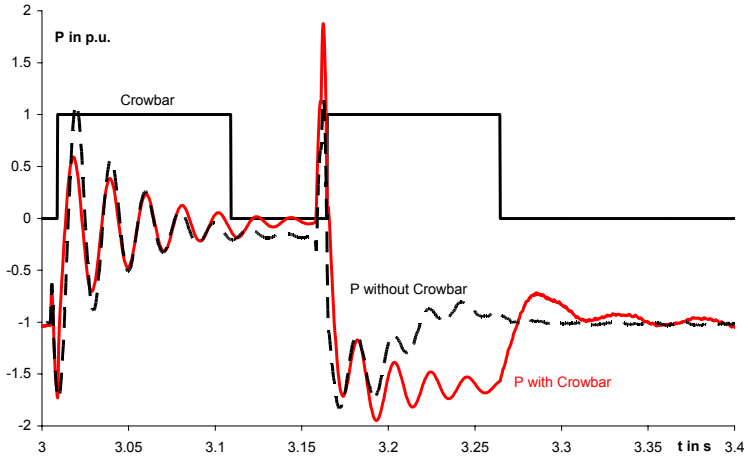

Figure 8: Comparison of real power output with and without crowbar

As can be seen in the plots (Figure 8 and Figure 9), the crowbar somewhat shaves the spikes occurring immediately after fault inception and later after fault clearance. As far as the real power output is concerned, no fundamental difference is to be observed as a result of the crowbar. The effect of the crowbar is more pronounced as regards the reactive power output.

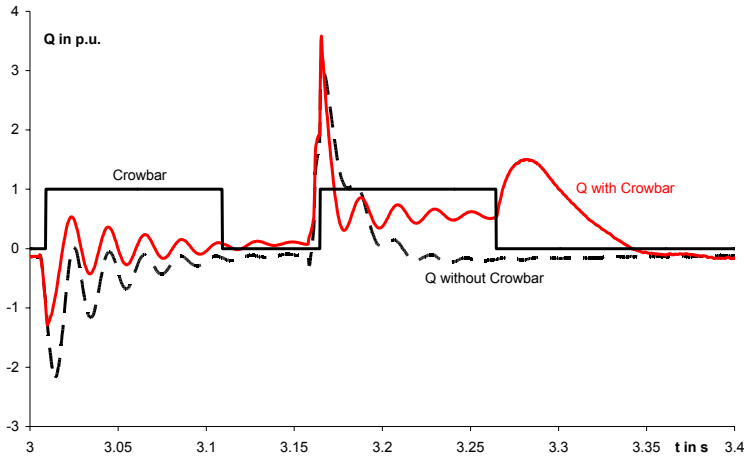

Figure 9: Comparison of the reactive power with and without crowbar

The crowbar significantly reduces the rotor currents during fault, as can be seen in Figures 10 a) (without crowbar) and 10 b) (with crowbar).

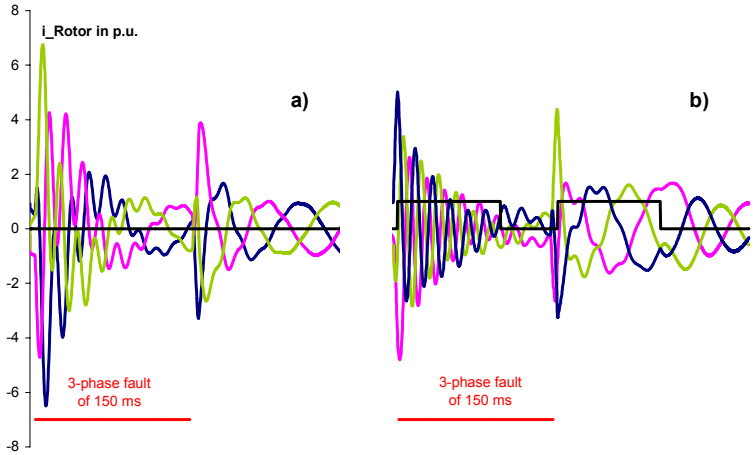

Figure 10 a, b: The rotor current during fault without crowbar

Discussion of the results

The most obvious conclusion to be deduced from the results obtained in this study is the fact that the reactive power output of the machine changes significantly after the second switching of the crowbar. In fact, the machine resorts to a net reactive power consumer from a situation where it would have been a net reactive power supplier without the crowbar. For the machine under consideration and for the given pre-fault condition, the duration of this unfavourable reactive power flow is about 0.15 s. However, this situation takes place immediately after fault clearance and can impede the post-fault voltage recovery process. As such, from the point of view of the network, the second switching of the crowbar has to be considered undesirable. If the switching still proves to be necessary, it will probably call for counter measures to avoid a voltage sag in the grid. The grid-side converter – with the control system appropriately designed to supply the necessary reactive power - may provide the solution. Another alternative is the static var compensator. On cost grounds, the latter option is likely to be a viable solution only in large wind parks.

CONCLUSION

The quasi-stationary model disregards the fundamental frequency transients in the machine currents. As a result, the model does not give the full picture with regard to currents in the converter and can lead to incorrect prediction of the sequence of crowbar actions. On the other hand, the use of the 5^{th} order model for a network of any practical size would still be quite a challenging computational task in spite of the immense computing capability available today.

To reconcile these two conflicting requirements, the approach adopted in this study was the simulation of the external network using its Thevénin equivalent when the DFIM is modelled in detail to capture the fast transients. This kind of modelling can be used when the main objective is the development and testing of single units.

For studies focussing primarily on the interaction of the DFIM with a large network on which the machine is operating, the authors are of the opinion that the quasi-stationary model is adequate.

Simulations on the crowbar action have revealed that the second switching of the crowbar after fault clearance affects the reactive power output of the machine significantly. Without a counter measure, this reactive power flow pattern can impede the voltage recovery in the network after fault. To assess its

full extent and to explore the possible remedial measures, the crowbar behaviour will be incorporated into the quasi-stationary model in the subsequent phase of the study.

NOMENCLATURE

Variables and constants

$\underline{u}$	voltage phasor in arbitrary reference frame
$\underline{i}$	current phasor in arbitrary reference frame
Ψ	flux-linkages
ω_0	radian frequency
ω_K	angular speed of an arbitrary reference frame
m_T	turbine torque
T_m	inertia constant

Subscripts/superscripts

R	rotor
S	stator
h	main field
σ	leakage
*	complex conjugate

Appendix

$$\alpha_T = l_h \cdot \left(\mathrm{Re}\{\underline{y}_{22}\} \cdot \mathrm{Im}\{\underline{y}_{12}\} - \mathrm{Re}\{\underline{y}_{12}\} \cdot \mathrm{Im}\{\underline{y}_{22}\}\right)$$

$$a = u_s \cdot \left(\mathrm{Re}\{\underline{y}_{22}\} \cdot \mathrm{Im}\{\underline{y}_{11}\} - \mathrm{Re}\{\underline{y}_{11}\} \cdot \mathrm{Im}\{\underline{y}_{22}\}\right)$$

$$b = u_s \cdot \left(\mathrm{Re}\{\underline{y}_{12}\} \cdot \mathrm{Re}\{\underline{y}_{21}\} + \mathrm{Im}\{\underline{y}_{12}\} \cdot \mathrm{Im}\{\underline{y}_{21}\} - \mathrm{Re}\{\underline{y}_{11}\} \cdot \mathrm{Re}\{\underline{y}_{22}\} - \mathrm{Im}\{\underline{y}_{11}\} \cdot \mathrm{Im}\{\underline{y}_{22}\}\right)$$

$$\beta_T = \sqrt{a^2 + b^2} \;\; , \;\; \delta_T = \tan^{-1}(b/a)$$

$$\gamma_T = {u_s}^2 \cdot \left(\mathrm{Re}\{\underline{y}_{21}\} \cdot \mathrm{Im}\{\underline{y}_{11}\} - \mathrm{Re}\{\underline{y}_{11}\} \cdot \mathrm{Im}\{\underline{y}_{21}\}\right) \cdot l_h$$

$$\alpha_{Syn} = -\frac{r_s \cdot x_h^2}{\omega_0 \cdot r_R^2 \cdot (r_s^2 + x_s^2)} \;\; ; \;\; \beta_{Syn} = \frac{u_s \cdot x_h}{\omega_0 \cdot r_R \cdot \sqrt{(r_s^2 + x_s^2)}} \;\; ; \;\; \delta_{Syn} = \frac{r_s}{x_s}$$

References

1. Koch, F.; Erlich, I.; Shewarega, F.: Dynamic Simulation of Large Wind Farms Integrated in a Multi Machine Network, IEEE PES General Meeting, Toronto, Canada, July 13-17, 2003
2. E.ON Netz GmbH: Netzanschlussregeln Hoch- und Höchstspannungsnetz, Bayreuth, 2003
3. Akhmatov, V.: Variable-speed Wind Turbines with Doubly-fed Induction Generators; part I: Modelling in Dynamic Simulation Tools, Wind Engineering Vol. 26, pp. 85-108 No.2, 2002
4. SEMIKRON innovation + service: IGBT Power Electronics Teaching System: Principe for sizing power converters, Application note
5. Akhmatov, V. Variable-speed Wind Turbines with Doubly-fed Induction Generators; part II: Power System Stability, Wind Engineering Vol. 26, pp. 171-188 No.3, 2002